AIAA JOURNAL
Vol. 34, No. 4, April 1996

Supersonic-Inlet Boundary-Layer Bleed Flow

Gary J. Harloff* and Gregory E. Smith†
NYMA, Inc., Brook Park, Ohio 44142

Boundary-layer bleed in supersonic inlets is typically used to avoid separation from adverse shock-wave–boundary-layer interactions and subsequent total-pressure losses in the subsonic diffuser and to improve normal-shock stability. Methodologies used to determine bleed requirements are reviewed. Empirical sonic flow coefficients are currently used to determine the bleed-hole pattern. These coefficients depend on local Mach number, pressure ratio, hole geometry, etc. A new analytical bleed method is presented to compute sonic flow coefficients for holes and narrow slots, and predictions are compared with published data to illustrate the accuracy of the model. The model can be used by inlet designers and as a bleed boundary condition for computational fluid-dynamic studies.

Nomenclature

A	= area
A_p	= porous area
A^*/A	= area ratio
C_b	= coefficient in Abrahamson's bleed model
C_d	= discharge coefficient
D	= bleed-hole diameter or hydraulic diameter
e_N, e_t	= unit vectors normal and tangential to surface
H_i	= incompressible boundary-layer shape factor, δ^*/θ
L	= bleed-hole plate thickness
M	= Mach number
p	= pressure
p_{t0}	= local total pressure at boundary layer edge
Q	= sonic mass-flow coefficient; ratio of actual to theoretical maximum mass flow at local total conditions
q	= dynamic pressure
R	= gas constant
Re	= Reynolds number
V_b, V_N	= bleed velocity normal to a wall
X_m	= p_a/p_0
$Xp(M_0, \theta)$	= function used in local-static-pressure model
γ	= ratio of specific heats, 1.4
ΔC_d	= discharge-coefficient change
δ^*	= boundary-layer displacement thickness
θ	= boundary-layer momentum thickness, or bleed-hole angle relative to local surface
ρ	= density
ϕ	= porosity

Subscripts

bl	= bleed
e	= boundary layer edge
pl	= bleed plenum
s	= static condition
t	= total condition
th	= theoretical
$0, a$	= freestream, ambient
1	= behind a normal shock
2	= bleed duct exit

Superscripts

L/D	= length/diameter
P	= pressure effect
w	= wall
$*$	= sonic

Received Jan. 4, 1995; presented as Paper 95-0038 at the AIAA 33rd Aerospace Sciences Meeting, Reno, NV, Jan. 9–12, 1995; revision received Oct. 27, 1995; accepted for publication Nov. 30, 1995.

*Senior Engineer II; currently consultant, North Olmsted, OH 44070. Associate Fellow AIAA.

†Research Engineer; currently consultant, Olmsted Falls, OH 44138. Senior Member AIAA.

Introduction

BOUNDARY-LAYER bleed in supersonic inlets is typically used to avoid boundary-layer flow separation from adverse shock-wave–boundary-layer interactions and subsequent total-pressure loss in the subsonic diffuser and to stabilize the normal shock. Currently bleed flow rates are determined from empirical sonic flow coefficients, which are measured in wind tunnels for specified Mach numbers and boundary-layer profiles. These coefficients depend on local Mach number, pressure ratio, hole or slot geometry, length-to-diameter ratio, etc. Because of scale effects relative to L/D and D/δ^*, these data may not readily scale to full scale. This paper reviews current boundary-layer bleed-removal design practice and to present a new analytical model for bleed-hole and narrow-slot sonic flow coefficients. Model predictions are compared with published test data to illustrate the accuracy of the model.

Inlet Bleed Considerations

Inlet boundary-layer bleed technology is both theoretical and empirical. Theoretical considerations enable the designer to compute viscous flowfields and boundary-layer characteristics and to determine bleed-band locations and bleed amounts. In addition, significant resources are needed to fine-tune the bleed bands during wind-tunnel experiments. Several studies are briefly reviewed to illustrate current practice.

Syberg and Hickcox[1] present a methodology to determine bleed-band locations and bleed flow rates for supersonic inlets. Boundary-layer profiles are determined, and values of the boundary-layer incompressible shape factor H_i are computed. Values of 1.3 correspond to fully developed profiles, and values between 1.8 and 2.0 correspond to profiles that are typically bled to avoid boundary-layer flow separation in regions of shock waves or diffused flow. The bleed bands are positioned to remove low-momentum boundary-layer flow near the wall to obtain acceptable incompressible shape factors over the mixed-compression operating range. To minimize bleed drag, 20-deg holes, relative to the local surface, are typically used on the centerbody and forward cowl bleed regions. In the throat region, 90-deg holes are used for normal-shock stability. Their diameters are sized so that $D/\delta^* = 1.0$. The authors noted that the boundary-layer growth rate increases in the bleed region because of surface roughness and mixing of high- and low-energy air in the boundary layer. Actual inlet bleed rates are typically 25% (Ref. 1) higher than theoretical bleed flow rates (computed to reduce H_i to acceptable

levels) to compensate for these roughness and mixing effects, which are difficult to model correctly. Recently Paynter et al.[2] addressed these issues with an increased near-wall roughness length scale in the algebraic turbulence model of Cebeci and Chang,[3] which correlates with the bleed mass flow. The roughness length scale is determined as a function of bleed rate, boundary-layer thickness, and bleed-hole diameter.

Tjonneland[4] indicates that the required inlet bleed decreases with increasing inlet scale because smaller inlet models tend to have larger-D/δ^* bleed holes. This larger D/δ^* increases the boundary-layer growth rate across bleed regions due to vortex shedding from the bleed holes. Values of D/δ^* of 0.5 in the forward cowl region and 1.0 in the throat region are typical of full scale. Values of D/δ^* of 2 on small-scale inlet models require higher bleed rates. Sonic flow coefficients Q are presented for $\frac{1}{6}$-scale and full-scale supersonic transport inlets for a design M_0 of 2.7. The L/D of the bleed holes is 4.8–5.6 for the $\frac{1}{6}$-scale model and 2.2–2.9 for the full-scale inlet. Thus scaling parameters for L/D and D/δ^* are identified. At cruise the predicted total inlet bleed drag for the four inlets (total bleed rate 13.6% of capture flow) represents a loss in range of 6%.

Bowditch[5] develops a linear correlation of (boundary-layer bleed)/(capture flow) vs (wetted area)/(throat area) for several two-dimensional and axisymmetric inlets for M_0 of 2.5–3.5. Bleed rates as high as 14% of capture flow are reported at 40% (wetted area)/(throat area). A typical inlet boundary-layer bleed schedule vs Mach number is specific by Hewitt and Johnston[6] and indicates that the bleed flow removal increases with Mach number. For example, at Mach 2.5 about 2.5% of capture flow is removed, and at Mach 7 about 14% is removed. These references provide only guidance; the location and amount of bleed required for a given inlet is determined empirically in a wind tunnel. For example, during a recent Mach 5 inlet test, Weir[7] indicates that about 40% of the wind-tunnel time was devoted to bleed optimization studies.

Wong[8] reports successful suppression of shock-induced boundary-layer separation with a bleed rate of up to 3% of capture flow for a normal shock of $M_0 = 1.9$. The bleed system is compartmentalized, has 30% porosity, and has normal holes of diameter δ^*. Continuous bleed upstream and through the shock-wave–boundary-layer interaction region is needed. He proposed a bleed criterion whereby the local boundary-layer total pressure minus the normal-shock total-pressure loss has to be greater than the downstream static pressure to avoid boundary-layer flow separation. Boundary-layer flow with total pressure less than this critical value should be removed. From M_e of 1.37–3.0 the relationship of M_{critical} vs M_e is linear. For example, at M_e of 3.0 the critical Mach number is 2.71, and at 1.37 the critical Mach number is 1.09. For the latter case, all boundary-layer flow below Mach 1.09 would be removed to satisfy this bleed criterion. Thus this method provides another criterion to select the amount of bleed needed to prevent boundary-layer flow separation at shock-wave impingement locations.

The following points summarize the above studies:

1) Bleed zones are needed where $H_{12} \geq 1.8$.

2) Actual bleed rates typically exceed theoretical rates by 25%.

3) Scaling parameters include L/D, D/δ^*, etc.

4) Significant wind-tunnel resources are committed to bleed-band optimization.

5) Adequate boundary-layer bleeding is necessary to control adverse shock–boundary-layer interaction.

Prior Modeling Work

Several modeling approaches have been used to model the bleed flow in supersonic inlets. These approaches include using nozzle equations, Darcy's law for porous plates, and specifying the local sonic flow coefficient Q as a constant or by a table lookup procedure. In computational fluid dynamics (CFD) codes, the mass flux at the wall is usually required as a bleed boundary condition, which can either be specified as a constant within a bleed band or allowed to vary with local flow conditions.

Abrahamson[9] modeled the bleed velocity V_b across the plate using a nozzle equation. For unchoked flow, $P_{\text{pl}}/P_{t0} > 0.528$,

$$V_b = \frac{C_b p_{\text{pl}} A_p}{\rho_w \sqrt{T_w}} \times \sqrt{\left(\frac{p_{t_w}}{p_p l}\right)^{(\gamma-1)/\gamma} \left[\left(\frac{p_{t_w}}{p_p l}\right)^{(\gamma-1)/\gamma} - 1\right] \frac{2\gamma}{R(\gamma-1)}} \tag{1}$$

For choked flow, $P_{\text{pl}}/P_{t_w} \leq 0.528$,

$$V_b = \frac{C_b p_{t_w} A_p}{\rho_w \sqrt{T_{t_w}}} \sqrt{\frac{\gamma}{R}} \left(\frac{\gamma+1}{2}\right)^{(\gamma+1)/2(\gamma-1)} \tag{2}$$

where C_b was assumed to be 0.2. The tangential velocity was assumed to be zero. This model ignores the effect of the aerodynamic controlling area or vena contracta on the flow velocity. This model is believed to be inadequate to model the velocity through short orifices with $L/D < 3$. It is a hypothesis of the present paper that flow through bleed holes is better modeled as orifice flow.

Benhachmi et al.[10] experimentally determined that, for a porous surface, the flow correlation developed for low-velocity normal flow also applied for parallel flow at Mach numbers of 2.5 and 3.0. The pressure drop through the porous material was modeled as a function of velocity squared, e.g.,

$$\frac{\Delta p}{\rho V_b^2} = 212.70 + \frac{7588.0}{Re} \tag{3}$$

where Re is based on the thickness of the porous material. This equation is not appropriate to model the flow through a bleed plate with discrete holes.

Chokani and Squire[11] used a linear Darcy-law equation to compute bleed velocity through a plate with holes. The equation was developed in a calibration rig, and used to compute flow through a bleed plate at transonic Mach numbers. The equation is

$$V_b/U_0 = 0.4\sqrt{\Delta p/\rho U_0^2} \tag{4}$$

The calibration-rig data were linear over the Δp range of the experiment from 700 to 4000 Pa, and nonlinear at higher values of Δp. In the development of this equation for transonic-flow application, the effects of boundary-layer displacement thickness, local Mach number, and compressibility have been ignored. The empirical nature of the curve fit over a limited range in Δp indicates that more research is needed to develop an improved correlation to cover a broader range of conditions.

Rallo[12] also used Darcy's law to model flow through four different porous plates at $M_0 = 6$. The equation is

$$\frac{V_b}{U_0} = \frac{\sigma}{\rho_0 U_0^2} \Delta p \tag{5}$$

where σ was varied from 0.1 to 0.3. The porosity varied from 22 to 28%. The uncertainty in the value of σ indicates that further research is needed for this method.

Mayer and Paynter[13] recently modeled the bleed boundary condition by computing the wall normal mass flow based on local flow properties, total bleed-hole area, and empirical sonic flow coefficients. The study used empirical data on the sonic flow coefficient for 90- and 20-deg holes from Syberg and Hickcox[1] and McLafferty and Ranard,[14] respectively. These coefficients are obtained by a table-lookup procedure at each boundary grid point in the bleed region. This procedure is limited by the range of the empirical data in the table.

Chyu et al.[15] investigated nine different bleed boundary conditions for CFD simulations of supercritical flow through an axisymmetric inlet at $M_0 = 2.65$. Three boundary conditions were used successfully to stabilize the terminal shock downstream of the inlet throat. Two of these did not utilize experimental pressure data. For choked bleed, the preferred boundary condition used:

$$V_N = C_d \sqrt{\gamma p/\rho} \tag{6}$$

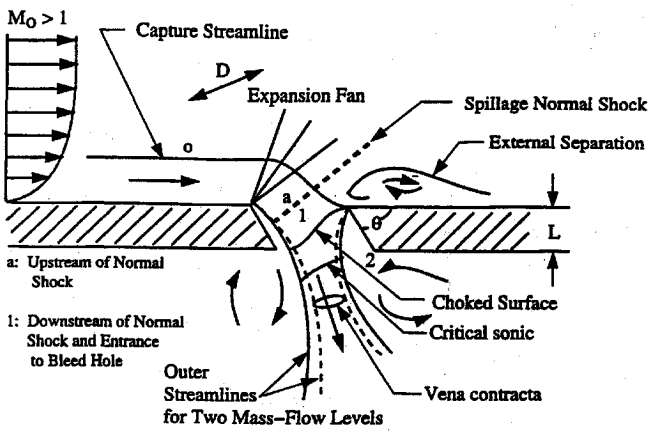

Fig. 1 Schematic of flow through angled bleed hole, centerline, $\theta > 50$ deg.

where the two models assumed either $C_d = 0.07$ or $C_d = 0.025 + 0.065\boldsymbol{e}_N \cdot \boldsymbol{e}_t$. This model does not have wide applicability.

In summary, there is not yet an accepted analytical bleed model.

New Bleed Model: Hole or Narrow Slot

A new bleed modeling approach is presented, which is based on conservation of mass, momentum, and energy for flow through a single hole or slot and empirical relations. An ideal gas is assumed with a ratio of specific heats of 1.4. The approach permits the local sonic flow coefficient to vary with local flow conditions, hole or slot geometry, and orientation.

The bleed duct is modeled like a pitot inlet with a detached normal shock when the boundary-layer edge Mach number is supersonic. For low-L/D orifices, $L/D \leq 3$, the minimum aerodynamic area is downstream of the orifice and is called a vena contracta. Sonic flow first occurs within the vena contracta; decreasing the downstream pressure will move the vena contracta toward the low-L/D orifice. This is indicated in Fig. 1 as the critical sonic line. When the Mach 1 surface reaches the orifice, the flow is only influenced by the upstream flow conditions, and this is indicated as the choked surface in Fig. 1. The outer streamlines indicate two levels of flow through the orifice. The dashed streamlines correspond to a smaller flow rate where the vena contracta is the controlling area, and the solid streamlines correspond to a larger mass flow rate where the critical sonic or choked surface is the controlling area. For high-L/D orifices, $L/D > 6$, the vena contracta is within the orifice and the flow chokes without an appreciable increase in the vena contracta area. Thus low-L/D orifices can increase the flow after reaching Mach 1 flow, whereas the longer orifices do not appreciably increase the flow after reaching Mach 1. Friction losses are associated with finite-length holes or slots. These losses have been modeled using Fanno friction losses, but for simplicity the losses are allowed for by a decrease in C_D for $L/D > 3$. Effects of M_0, p_2/p_0, L/D, and θ are modeled empirically.

The flow through a low-L/D orifice, of angle θ, is shown schematically in Fig. 1, with supersonic local flow. Boundary-layer flow separation is indicated on both sides of the orifice, and a spillage normal shock is detached. The internal and external flowfield communicate through the separated boundary layer until the vena contracta moves into the orifice. Stations used in the model are identified in Fig. 1. Computational fluid dynamics studies by Chyu et al.[16] have illustrated a similar shock structure as indicated in Fig. 1 for a 90-deg hole and indicated that boundary-layer flow separation is present for 90-deg holes and not for 30-deg holes. Boundary-layer separation inside a 90-deg bleed slot has been reported by Hahn and Shih[17] and Davis et al.[18]

Model for the Sonic Flow Coefficient

Simple one-dimensional gasdynamic relationships are used to obtain an expression for the theoretical sonic flow coefficient.

The ratio of freestream total to static pressure is

$$(p_t/p_s)_0 = \left(1 + 0.2M_0^2\right)^{3.5} \tag{7}$$

If $M_0 \cos\theta > 1$ and $\theta > 50$ deg, the normal-shock pressure jump is

$$\frac{p_1}{p_a} = \frac{7(M_0 \cos\theta)^2 - 1}{6} \tag{8}$$

The ratio of exit static to local static pressure is

$$p_2/p_0 = (p_2/p_{t_0})(p_{t_0}/p_a)(p_a/p_0) \tag{9}$$

where p_a/p_0 allows for a reduction in static pressure from station 0 to station a (see Fig. 1 and the Local Static Pressure subsection below). For $\theta > 50$ deg, $p_a/p_0 = 1.0$.

The bleed-hole exit Mach number is

$$M_2 = \sqrt{5(p_2/p_0)^{-\frac{2}{7}} - 5} \qquad M_2 \leq 1 \tag{10}$$

where p_0 is assumed to be the effective local total pressure at station 2. If friction losses are computed, then p_{t2} will be computed. The ratio A^*/A at the bleed-hole exit is

$$(A^*/A)_2 = (216/125)M_2\left[1 + 0.2M_2^2\right]^{-3} \tag{11}$$

The sonic exit area is

$$A_2^* = A_{\text{bl}}(A^*/A)_2 \tag{12}$$

The exit mass flow is

$$w_2 = 0.532\, A_2^* p_0/\sqrt{T_{t0}} \tag{13}$$

For hole angles other than 90 deg there is a ram effect as described in the Ram Effect subsection below.

The sonic flow rate is

$$w^* = 0.532 A_{\text{bl}}\, p_{t0}/\sqrt{T_{t0}} \tag{14}$$

The theoretical sonic flow coefficient Q_{th} is

$$Q_{\text{th}} = w_2 C_d / w^* \tag{15}$$

where $C_d = C_d\,(C_{d0}, p_2/p_0, \theta, M_0, L/D, \ldots)$ and w^* is the sonic flow rate at local total pressure and total temperature. The Bragg[19] model is used to determine the pressure-ratio dependence of the discharge coefficient. The empirical relations developed for $C_d(\theta, M_0)$ were developed using the single-hole experimental data of Davis et al.[20]

Compressible Discharge Coefficient

The discharge coefficient is assumed above to depend on the pressure ratio p_2/p_0; the bleed-hole angle relative to the local surface, θ; the local Mach number M_0; the orifice L/D; etc. The model for C_d is developed below.

Vena Contracta Effect

Studies by Jobson[21] provide an analytical framework for the modeling the variation of the vena contracta area ratio with the pressure ratio p_2/p_0. He assumed that the velocity profile upstream and parallel to the orifice centerline was independent of flow rate, and this is also assumed here for $M_0 = 0.0$. Bragg[19] extended Jobson's analysis procedure to allow for compressibility effects, and the Bragg analysis is used to determine a baseline discharge coefficient of the orifice. The discharge coefficient is equal to the vena contracta area divided by the orifice area. The details can be found in Bragg.[19] This C_d is then modified empirically to allow for M_0, L/D, and θ effects. Briefly, the Bragg model, $C_d(p_2/p_0, \theta)$, is the basis for the discharge coefficient, and increments in C_d are assumed to be linear in view of the effects of convection (M_0), internal flow separation (p_2/p_0), separation for $\theta > 50$ deg, and friction (L/D). The details of the C_d buildup, or increments, are given below and are summarized in Table 1.

Table 1 Model for discharge coefficient C_d and buildup ΔC_d

Design space	$C_d = C_d(p_2/p_0, \theta) + \Delta C_d^P + \Delta C_d^* + \Delta C_d^{L/D}$	Effect modeled
Baseline	$C_d(p_2/p_0, \theta)$	Bragg model
$M_0 = 0$, 90-deg hole	$C_{d0} = 0.82$	Geometry-dependent; no internal separation
$M_0 = 0$	$C_d = C_{d0} + \Delta C_d^{L/D}$	No convection effect
$0 < M_0 < 0.6$	$C_d = (C_{d0} + C_d)/2$	Convection effects
	See Fig. 3	Flow separation due to M_0^0, $\theta = 90$ deg:
$0 < M_0 \leq 0.6$	$\Delta C_d^*(M_0) = -0.1 M_0$	Sonic C_d correction: convection effects
$0.6 < M_0 \leq 1.0$	$\Delta C_d^*(M_0) = -0.06 - 0.4(M_0 - 0.6)$	Separation starting
$1.0 < M_0 \leq 1.6$	$\Delta C_d^*(M_0) = -0.22 - 0.217(M_0 - 1.0)$	Shock effect on separation
$M_0 > 1.6$	$\Delta C_d^*(M_0) = -0.35$	Separation profile self-similar
		Pressure ratio:
$M_0 > 0.84$, $p_2/p_0 > 0.5$, $\theta > 50$ deg	$\Delta C_d^P = -0.46(p_2/p_0 - 0.5)$	Internal flow separation
Otherwise	$\Delta C_d^P = 0.0$	No separation
		Bleed-hole angle effect:
$\theta \geq 50$ deg	$\Delta C_d^* = \Delta C_d^* \frac{\partial C_d^*}{\partial \theta} \Delta\theta$	Flow separation, $\theta < 90$ deg
	$\frac{\partial C_d^*}{\partial \theta} = \frac{1 - 0}{90 \text{ deg} - 50 \text{ deg}} = 0.025$	
$\theta < 50$ deg	$\Delta C_d^* = 0$	No separation
		L/D, hole or slot:
Hole, $L/D < 3$	$\Delta C_d^{L/D} = 0.08$	Hole is baseline
Hole, $L/D \geq 3$	$\Delta C_d^{L/D} = 0.00$	Internal friction loss
Slot, $L/D < 3$	$\Delta C_d^{L/D} = 0$	Slot has more boundary-layer separation loss than hole
Slot, $L/D \geq 3$	$\Delta C_d^{L/D} = -0.08$	Internal friction loss

Recall that the pressure ratio across the orifice is increased by a normal-shock pressure jump (at freestream Mach number), where $\theta \leq 50$ deg; see (9). When $\theta > 50$ deg a normal shock is absent.

If $M_0 = 0$, then $C_d = C_{d0}$, where $C_{d0} = 0.82$ for holes and 0.74 for narrow slots. The constant C_{d0} at $M_0 = 0$ is based on the assumption that the velocity profile into the orifice is independent of pressure ratio. For $0 < M_0 \leq 0.6$ the orifice discharge coefficient is an average of C_{d0} and C_d computed by the model.

Flow Separation

The sonic discharge coefficient decreases with increasing freestream, or boundary-layer edge, Mach number as shown in Fig. 2. The relationship is approximated over three zones. For subsonic flow, $0.0 < M_0 \leq 0.6$, a gradual reduction in C_d^* is observed, probably because of convection effects on the inlet velocity profiles. The sharper reduction in C_d^*, for $0.6 < M_0 \leq 1.6$ is thought to be a result of boundary-layer flow separation outside and/or inside the bleed hole (slot). Above $M_0 = 1.6$ the separation pattern is apparently self-similar. These relationships are empirically determined using the mathematical model to determine differences in sonic C_d^* with M_0 and experimental data. The relationships of ΔC_d^* vs M_0 are listed in Table 1.

Pressure-Ratio Effect

The discharge coefficient is reduced to allow for internal flow separation. For bleed-hole angles greater than 50 deg, pressure ratios, $p_2/p_0 \geq 0.5$, and local Mach numbers greater than 0.84,

$$\Delta C_d^P = -0.46[(p_2/p_0) - 0.5] \tag{16}$$

otherwise $\Delta C_d^P = 0.0$. The 50-deg limit for internal flow separation is based on the observation that empirical corrections [e.g., (16)] change for smaller angles. These equations are probably dependent on the radius of the hole edges, etc.

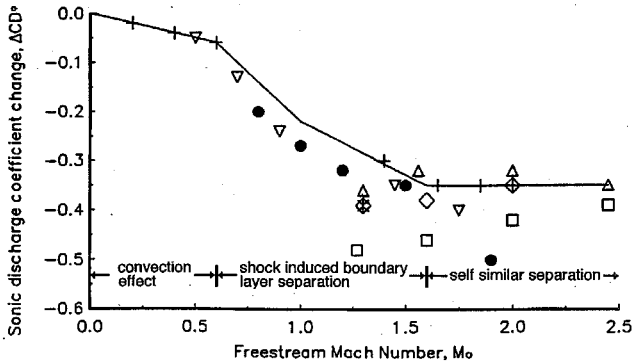

Fig. 2 Sonic discharge coefficient decrease vs Mach number, $\theta = 90$ deg: +, Davis et al.,[20] $L/D = 2$ single hole; ⊥, Davis et al.,[20] $L/D = 1$, single hole; ◇, Willis et al.,[25] slot, $L/D = 1$; △, Willis et al.,[25] $L/D = 1$, plate; □, Willis et al.,[25] slot, $L/D = 2.54$; ▽, McLafferty,[14] $L/D = 6$, plate; ●, Syberg and Koncsek,[23] $L/D = 3$, plate; and ——, equation; see Table 1.

Hole-Angle Effect

The reduction in C_d is assumed to be zero for $\theta \leq 50$-deg holes, or narrow slots, and linear for larger angles. A narrow slot is one with $D/\delta^* \sim 1$; the range in D/δ^* for this model to be valid is unknown. The equation follows:

$$\text{slope}|_\theta = \frac{\partial C_d}{\partial \theta} = \left(\frac{1 - 0}{90 \text{ deg} - 50 \text{ deg}}\right) = 0.025 \tag{17}$$

$$\Delta C_d^\theta(p_2/p_0, \theta) = \Delta C_d^P(0.025)\,(\theta - 50 \text{ deg}); \quad 50 \text{ deg} \leq \theta \leq 90 \text{ deg} \tag{18}$$

$$\Delta C_d^\theta(p_2/p_0, \theta) = 0; \qquad \theta < 50 \text{ deg} \tag{19}$$

It is hypothesized that, for $M_0 \cos\theta > 1$ and $\theta \geq 50$ deg, internal and external boundary-layer flow separation are coupled aerodynamically until the flow is choked. This phenomenon may be responsible for the increase in turbulence previously ascribed to roughness.

Ram Effect

For 90-deg bleed holes, the bleed entrance total pressure is the local freestream static pressure. For hole angles less than 90 deg the total pressure at the bleed-hole entrance is assumed to be proportional to the dynamic pressure, at the boundary-layer edge, directed into the bleed hole (or slot) and to any normal-shock total-pressure loss, i.e.,

$$q/p_0 = (\gamma/2)\,\text{const}(\theta)\,(M_0\cos\theta)^2(p_{t1}/p_{t_0}) \tag{20}$$

where the loss in total pressure resulting from a normal shock for $M_0 > 1$ is

$$\frac{p_{t1}}{p_{t0}} = \left(\frac{6M_0^2}{M_0^2+5}\right)^{3.5}\left(\frac{6}{7M_0^2-1}\right)^{2.5} \tag{21}$$

The upstream Mach number is assumed to be M_0, and

$$w_2 = 0.532A_{s2}p_0[1 + (q/p_0)](1/\sqrt{T_{t0}}) \tag{22}$$

The function const(θ) is

θ, deg	const(θ)
0	1.0
20	0.7
40	0.2
90	0.0

A curvefit of const(θ) vs θ can be used to determine values of const(θ) for other values of θ, or one may use const(θ) = $\cos^6\theta$.

Local Static Pressure

The bleed entrance static pressure is assumed to decrease with increasing M_0 for low bleed-hole (or slot) angles θ as the flow accelerates through the turn. The pressure reduction begins at $M_0 = 0.2$ and continues until $M_0 = 1.2$, and is constant above $M_0 = 1.2$. The equation used is

$$X_M = p_a/p_0 = 1.0; \qquad 0 < M_0 \leq 0.2 \tag{23}$$

$$X_M = 1.0 + \left(\frac{XP(M_0,\theta) - 1.0}{1.2 - 0.2}\right)(M_0 - 0.2); \qquad 0.2 < M_0 < 1.2 \tag{24}$$

$$X_M = XP(M_0,\theta); \qquad M_0 \geq 1.2 \tag{25}$$

where $XP(M_0, \theta)$ is

θ, deg	M_0	$XP(M_0,\theta)$
90	$\neq 1$	1.0
40	< 1	0.75
40	≥ 1	1.0
20	$\neq 1$	0.75

Interpolation is required for other hole (or slot) angles.

***L/D* Effect**

For L/D of 3 or greater the C_d is reduced by 0.08 to allow for the higher friction loss in the larger passage configuration. Also, for narrow slots with low L/D, the C_d is lowered by 0.08 to allow for added separation losses over the hole configuration. Alternatively, friction effects have been modeled as a Fanno friction loss that reduces the exit total pressure and mass flow. In the interest of simplicity the L/D losses are, for the present time, modeled as a constant decrease in C_d.

Comparison with Test Data

The data on a single 90-deg bleed hole with diameter $\frac{1}{8}$ in., taken by Davis et al.,[20] were modeled. Figures 3 and 4 cover subsonic and supersonic flow with Mach-number ranges 0.0–0.6 and 1.4–2.0, respectively. As the local edge Mach number increases, the sonic flow coefficient Q decreases as a result of A^* decreasing. The predicted bleed rates are in good agreement with the test data for both subsonic and supersonic Mach numbers. The test data and the analytical predictions can also be collapsed onto subsonic and supersonic curves by normalizing the flow coefficient by the product of p_{t0}/p_0 and p_{t1}/p_{t0} and plotting vs $(p_0 - p_2)/p_{t0}$; see Fig. 5. This feature suggests that a normal shock is present for supersonic edge Mach numbers. Smith[22] first suggested plotting Qp_{t0}/p_0 vs $(p_0 - p_2)/p_{t0}$.

Experimental and analytical 20-deg single-hole bleed data of Davis et al.[20] are shown in Fig. 6 over the Mach-number range from 0.0 to 2.0. The analytical model compares well with the data.

Similar bleed flow-rate data for multihole bleed-plate tests for Mach 0.8 to 2.2, from Syberg and Koncsek,[23] are illustrated in Figs. 7, 8, and 9 for 90-, 40-, and 20-deg holes, respectively. The data in Fig. 7 are originally from Dennard[24] and McLafferty.[14] The single-hole model predictions compare reasonably well with the multiple-hole test data, with the supersonic data modeled more accurately than the transonic data. Flow separation effects are modeled for bleed-hole angles $\theta > 50$ deg and are not modeled for $\theta < 50$ deg.

The test data of McLafferty and Ranard[14] are compared with model predictions for 90-, 40-, and 20-deg multiple holes in Figs. 10, 11, and 12, respectively. The plates used had two rows of holes.

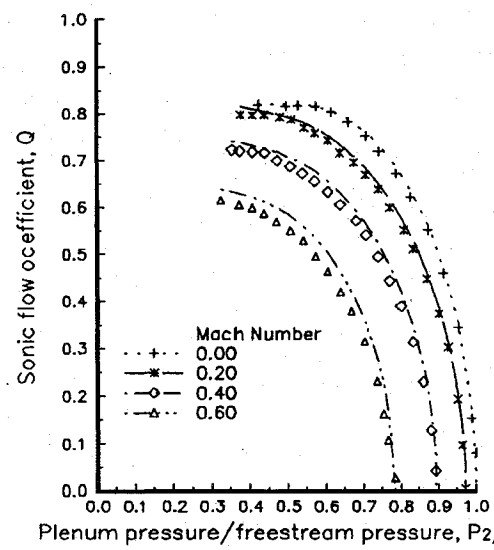

Fig. 3 Sonic flow coefficient, single 90 deg hole, *L/D* = 2 (test data of Davis et al.[20]): symbols, test data and lines, model.

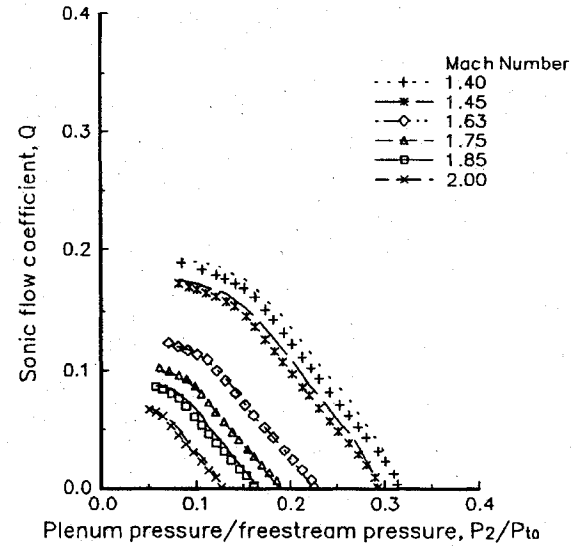

Fig. 4 Sonic flow coefficient, single 90 deg hole, *L/D* = 2 (test data of Davis et al.[20]).

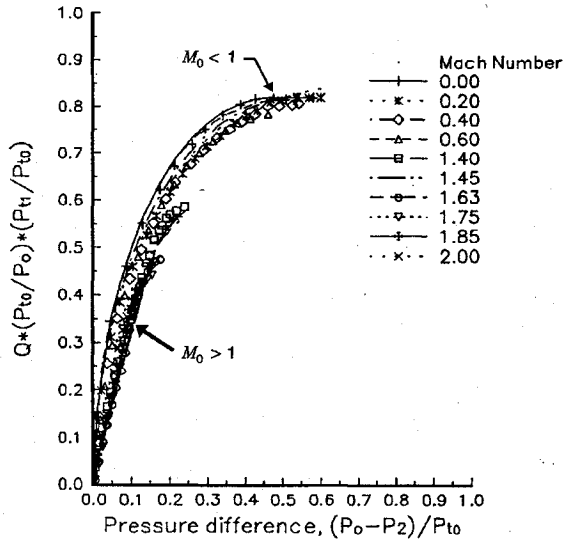

Fig. 5 Sonic flow coefficient, single 90 deg hole, $L/D = 2$ (test data of Davis et al.[20]).

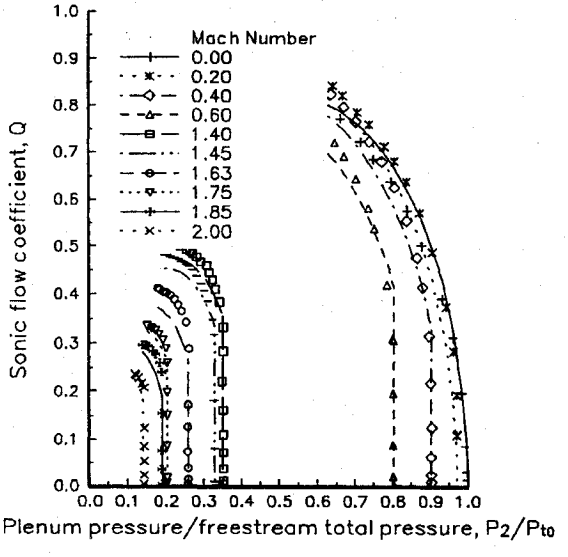

Fig. 6 Sonic flow coefficient, single 20 deg hole, $L/D = 2$ (test data of Davis et al.[20]).

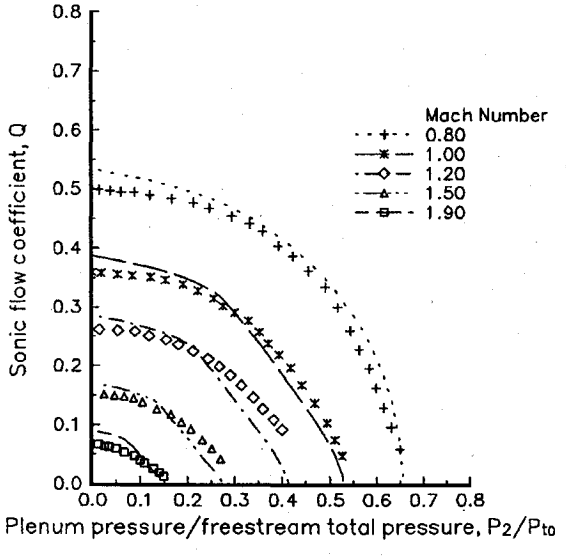

Fig. 7 Sonic flow coefficient, 90-deg plate, $L/D = 3$ (test data of Syberg and Koncsek,[23] Dennard,[24] and McLafferty and Ranard[14]).

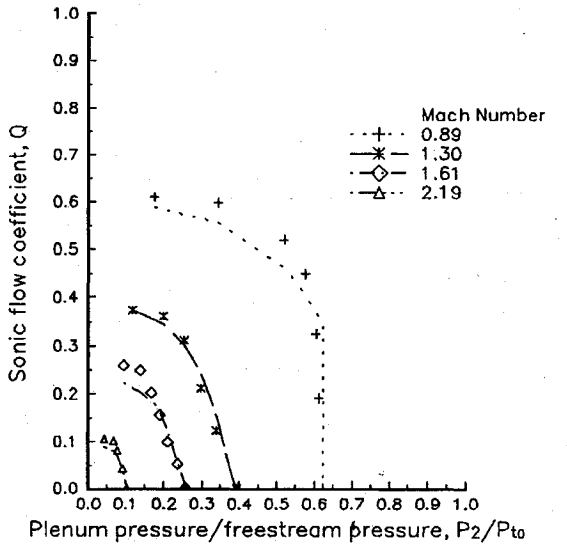

Fig. 8 Sonic flow coefficient, 40-deg plate, $L/D = 3$ (test data of Syberg and Koncsek[23]).

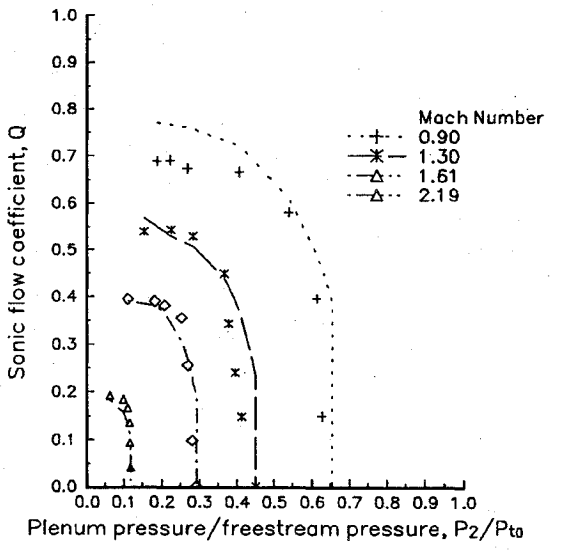

Fig. 9 Sonic flow coefficient, 20-deg plate, $L/D = 3$ (test data of Syberg and Koncsek[23]).

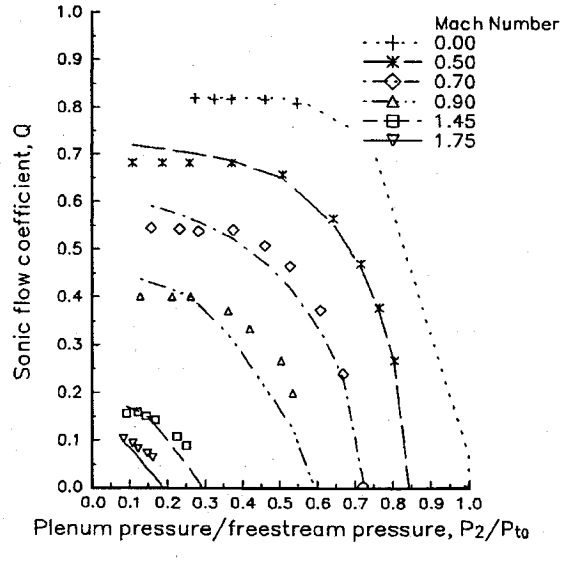

Fig. 10 Sonic flow coefficient, 90-deg plate, $L/D = 6$ (test data of McLafferty and Ranard[14]).

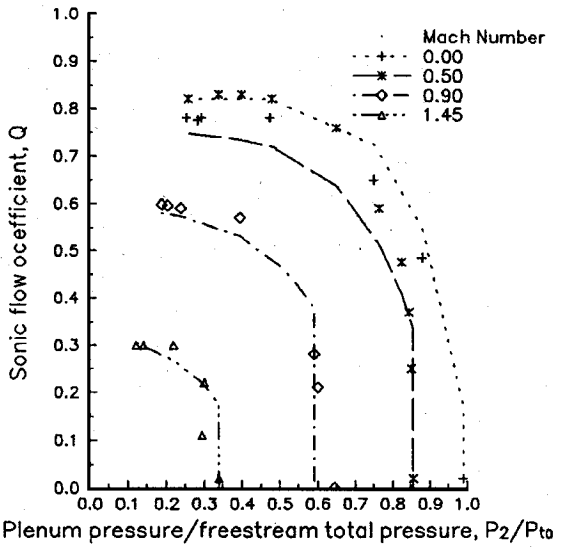

Fig. 11 Sonic flow coefficient, 40-deg plate, $L/D = 6$ (test data of McLafferty and Ranard[14]).

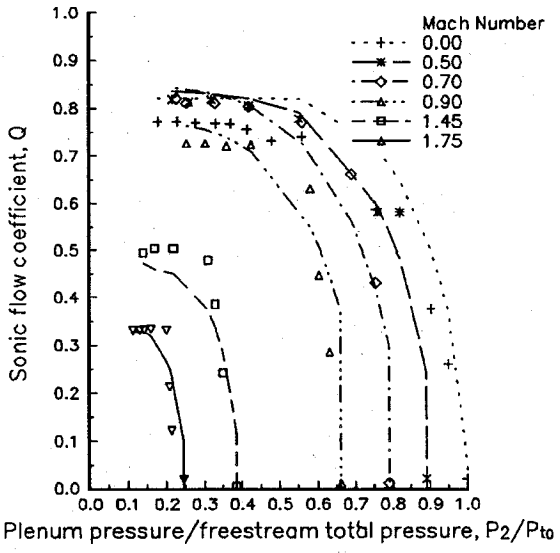

Fig. 12 Sonic flow coefficient, 20-deg plate, $L/D = 6$ (test data of McLafferty[14]).

These data are for L/D of 6.0, and the discharge coefficient was lowered by 0.08 as discussed previously. The agreement with the model results is encouraging.

Slot data at the same Mach numbers from Willis et al.[25] for M_0 from 1.27 to 2.46 are illustrated in Fig. 13. The slot is 1 cm wide and 1 cm deep. The agreement is good except at the nominal Mach 1.3 condition. Possible reasons for the discrepancies from $M_0 = 1.27$ to 1.37 are that the model $\Delta C_d^*(M_0)$ is not correct (see Fig. 2 and the equations in Table 1), the wind-tunnel M_0 not accurate, etc. The data scatter present in Fig. 2 is largest from $M_0 = 1.25$ to 2.0. More research is needed to better understand the data scatter. In general, the agreement with test data is similar to that for a hole, with better comparison at subsonic or supersonic speeds than transonic speeds.

A significant contribution of the analytical bleed model is that the original premise, that a single-hole model can be used to model multiple holes, has been validated. This suggests that smaller, more economical wind tunnels can be utilized to generate flow coefficient data. More aerodynamically efficient hole shapes are good candidates for single-hole testing. It is recognized that radiusing the holes or changing the hole entrance geometry will change the behavior of the flow rate vs pressure.

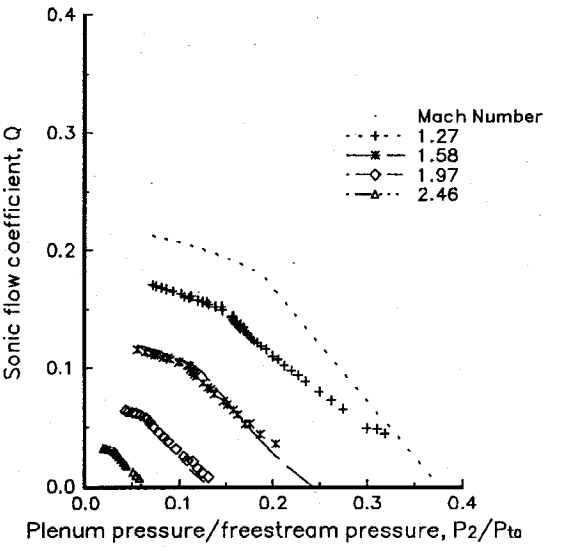

Fig. 13 Sonic flow coefficient, 90-deg slot, $L/D = 2.54$ (test data of Willis et al.[25]).

Conclusions

An analytical model for boundary-layer bleed holes and slots has been developed. The basis for the model is compressible flow through a single duct, with a model for the vena contracta that controls the aerodynamic area downstream of the duct in the plenum for short L/D holes or slots. Empirical adjustments were made to allow for L/D, M_0, and bleed-hole and slot-angle effects. The new model predictions compare well with most of the known existing test data for both holes and narrow slots at 90 deg, and for holes at 40 and 20 deg. The model should be useful to inlet designers and as a bleed boundary condition in CFD codes, where the bleed has to be computed from local flow conditions, the plenum pressure, and the hole or slot geometry.

Several insights were gained from the bleed model. For the 90-deg holes and narrow slots, ΔC_d^* gradually decreases from Mach number 0.0 to 0.6; thereafter it decreases more rapidly with increasing Mach number. Above $M = 1.6$, ΔC_d^* does not decrease further. This is interpreted as follows: at low subsonic Mach numbers, convection effects decrease the sonic flow coefficient. Boundary-layer flow separation in the holes or narrow slot begins at $M_0 = 0.6$ and increases until the edge Mach number reaches 1.6. At higher Mach numbers the boundary-layer flow separation pattern does not change. For holes and slots at angles less than 50 deg, three flow effects were modeled: 1) a ram effect was added to the inflow pressure, 2) the static pressure acting at the hole entrance was reduced, and 3) the decrease in $\Delta C_d^*(M_0)$ was set equal to zero, since there is no flow separation model needed inside the holes or slots. Because of the perceived boundary-layer flow separation present in bleed passages for $\theta > 50$ deg, there is an apparent opportunity to increase Q by providing more aerodynamically efficient flow passages. Flow coefficients are higher for holes than narrow slots, probably because of the more severe boundary-layer flow separation in slots.

Acknowledgments

This project was supported by NASA Lewis Research Center under Contract NAS3-27186. The manuscript preparation assistance of Tammy Langhals and Maryann Johnston is gratefully acknowledged.

References

[1]Syberg, J., and Hickcox, T. E., "Design of a Bleed System for a Mach 3.5 Inlet," NASA CR-2187, Jan. 1973.

[2]Paynter, G. C., Treiba, D. A., and Kheeling, W. D., "Modeling Supersonic Boundary-Layer Bleed Roughness," *Journal of Propulsion and Power*, Vol. 9, No. 4, 1993, pp. 622–627.

[3]Cebeci, T., and Chang, K. C., "Calculation of Incompressible Rough-Wall Boundary Layer Flows," *AIAA Journal*, Vol. 16, No. 7, 1978, pp. 730, 731.

[4]Tjonneland, E., "The Design, Development, and Testing of a Supersonic Transport Intake System," *Inlets and Nozzles for Aerospace Engines*, AGARD-CP-91-71, 1971, pp. 18-1–18-17.

[5]Bowditch, D. N., "Some Design Considerations for Supersonic Cruise Mixed Compression Inlets," NASA TM-71460, Nov. 1973.

[6]Hewitt, F. A., and Johnston, M. C., "Propulsion System Performance and Integration for High Mach Air Breathing Flight," *High-Speed Flight Propulsion*, edited by A. R. Seebass, Vol. 137, Progress in Astronautics and Aeronautics, AIAA, Washington, DC, 1991, pp. 101–142.

[7]Weir, L. J., NASA Lewis Research Center, Cleveland, OH, private communications, Sept. 1993.

[8]Wong, W. F., "The Application of Boundary Layer Suction to Suppress Strong Shock-Induced Separation in Supersonic Inlets," AIAA Paper 74-1063, Oct. 1974.

[9]Abrahamson, K. W., "Numerical Investigation of a Mach 3.5 Axisymmetric Inlet with Multiple Bleed Zones," AIAA Paper 88-2588, June 1988.

[10]Benhachmi, D., Greber, I., and Hingst, W., "Experimental and Numerical Investigation of the Effect of Distributed Suction on Oblique Shock Wave/Turbulent Boundary Layer Interaction," NASA TM-101334, Aug. 1988.

[11]Chokani, N., and Squire, L. C., "Transonic Shockwave/Turbulent Boundary Layer Interactions on a Porous Surface," *Aeronautical Journal*, Vol. 97, May 1993, pp. 163–170.

[12]Rallo, R. A., "An Investigation of Passive Control Methods for Shock-Induced Separation at Hypersonic Speeds," M.S. Thesis, Aerospace Dept., Univ. of Michigan, Ann Arbor, MI, 1992.

[13]Mayer, D. W., and Paynter, G. C., "Boundary Conditions for Unsteady Supersonic Inlet Analyses," ISABE 93-7104, pp. 1062–1070.

[14]McLafferty, G., and Ranard, E., "Pressure Losses and Flow Coefficients of Slanted Perforations Discharging from Within a Simulated Supersonic Inlet," R-0920-1, United Aircraft Corp., 1958.

[15]Chyu, W. J., Howe, G. W., and Shih, T. I.-P., "Bleed Boundary Conditions for Numerically Simulated Mixed-Compression Supersonic Inlet Flow," *Journal of Propulsion and Power*, Vol. 8, No. 4, 1992, pp. 862–868.

[16]Chyu, W. J., Rimlinger, M. J., and Shih, T. I-P., "Effects of Bleed-Hole Geometry and Plenum Pressure on Three-Dimensional Shock-Wave/Boundary-Layer/Bleed Interactions," AIAA Paper 93-3259, July 1993.

[17]Hahn, T. O., and Shih, T. I-P., "Numerical Study of Shock-Wave/Boundary-Layer Interactions with Bleed," *AIAA Journal*, Vol. 31, No. 5, 1993, pp. 869–876.

[18]Davis, D. O., Willis, B., and Hingst, W., "Flowfield Measurements of Slot-Bleed/Oblique Shock-Wave Interaction," AIAA Paper 95-0032, Jan. 1995.

[19]Bragg, S. L., "Effect of Compressibility on the Discharge Coefficient of Orifices and Convergent Nozzles," *Journal of Mechanical Engineering Science*, Vol. 2, No. 1, 1960, pp. 35–44.

[20]Davis, D. O., Hingst, W. R., and Bodner, J. P., "Flow Coefficient Behavior for Isolated Normal and 20 Degree Boundary Layer Bleed Holes," NASA TM 106816, 1995.

[21]Jobson, D. A., "On the Flow of a Compressible Fluid Through Orifices," *Proceedings of the Institute of Mechanical Engineering*, London, Vol. 169, No. 37, 1955, pp. 767–775.

[22]Smith, G. E., "Bleed Modeling," NASA Lewis Research Center, Workshop in Inlet Bleed Modeling, Sept. 1993.

[23]Syberg, J., and Koncsek, J. L., "Bleed System Design Technology for Supersonic Inlets," AIAA Paper 72-1138, Nov. 1972.

[24]Dennard, J. S., "A Transonic Investigation of the Mass-Flow and Pressure Recovery Characteristics of Several Types of Auxiliary Air Inlets," RM L57B07, NACA, 1957.

[25]Willis, B., Davis, D. O., and Hingst, W. R., "Flow Coefficient Behavior for Boundary Layer Bleed Holes and Slots," AIAA Paper 95-0031, Jan. 1995.